Ab initio scaling laws for the formation energy of nanosized interstitial defect clusters in iron, tungsten, and vanadium

R. Alexander,[1] M.-C. Marinica,[1] L. Proville,[1] F. Willaime,[2] K. Arakawa,[3] M. R. Gilbert,[4] and S. L. Dudarev[4]
[1]*DEN-Service de Recherches de Métallurgie Physique, CEA, Université Paris–Saclay, F-91191, Gif-sur-Yvette, France*
[2]*DEN-Département des Matériaux pour le Nucléaire, CEA, Université Paris–Saclay, F91191, Gif-sur-Yvette, France*
[3]*Department of Materials Science, Faculty of Science and Engineering, Shimane University, 1060 Nishikawatsu, Matsue 690-8504, Japan*
[4]*Culham Centre for Fusion Energy, Culham Science Centre, Abingdon, Oxfordshire OX14 3DB, United Kingdom*
(Received 14 April 2016; published 6 July 2016)

The size limitation of *ab initio* calculations impedes first-principles simulations of crystal defects at nanometer sizes. Considering clusters of self-interstitial atoms as a paradigm for such crystal defects, we have developed an *ab initio*–accuracy model to predict formation energies of defect clusters with various geometries and sizes. Our discrete-continuum model combines the discrete nature of energetics of interstitial clusters and continuum elasticity for a crystalline solid matrix. The model is then applied to interstitial dislocation loops with ⟨100⟩ and $1/2\langle 111\rangle$ Burgers vectors, and to C15 clusters in body-centered-cubic crystals Fe, W, and V, to determine their relative stabilities as a function of size. We find that in Fe the C15 clusters were more stable than dislocation loops if the number of self-interstitial atoms involved was fewer than 51, which corresponds to a C15 cluster with a diameter of 1.5 nm. In V and W, the $1/2\langle 111\rangle$ loops represent the most stable configurations for all defect sizes, which is at odds with predictions derived from simulations performed using some empirical interatomic potentials. Further, the formation energies predicted by the discrete-continuum model are reparametrized by a simple analytical expression giving the formation energy of self-interstitial clusters as a function of their size. The analytical scaling laws are valid over a very broad range of defect sizes, and they can be used in multiscale techniques including kinetic Monte Carlo simulations and cluster dynamics or dislocation dynamics studies.

DOI: 10.1103/PhysRevB.94.024103

I. INTRODUCTION

The ability of materials to sustain extreme conditions, encountered in fusion-plasma confinement reactors or in space exploration, depends on the formation and mobility of clusters of vacancies and interstitial atoms. As such, a study of defects in body-centered-cubic refractory metals and iron provides a foundation for future research in structural materials, and it paves the way for a better understanding of materials ageing. Over the lifetime of reactor components, the mobility of individual defects gives rise to clustering and growth of defect clusters. Vacancies and self-interstitial atoms (SIAs) form either two- or three-dimensional clusters, depending on their size, as a result of competition between the interface and bulk energies, as described by the Gibbs theory of wetting [1]. Vacancy cluster morphology of various bcc metals is fairly well known and exhibits similar behavior. There is a competition between planar loops and voids, as confirmed by experimental observations [2,3]. However, SIA clusters show acutely different properties depending on the bcc material under consideration.

Density functional theory (DFT) calculations and other *ab initio* methods provide quantitative insight into the nature of clusters containing a small number of defects. DFT calculations show that the most stable single SIA in Fe adopts a configuration that corresponds to a ⟨110⟩ dumbbell, whereas in other bcc transition metals, a single SIA forms a defect aligned along the ⟨111⟩ direction, known as a crowdion [4–7]. These DFT predictions broadly agree with experiment [8], which makes it desirable to extend predictions to clusters larger than a single SIA. Dumbbells can be packed together in bundles to form small dislocation loops. DFT predicts that in Fe the orientation of these dumbbells changes from ⟨110⟩ to ⟨111⟩ depending on the number of SIAs involved. The transition occurs at around five SIAs [9,10]. In Fe, observation of nanometric-sized clusters of SIAs by transmission electron microscopy (TEM) techniques reveals the presence of planar loops, which can adopt either the $1/2\langle 111\rangle$ (highly mobile) or ⟨100⟩ (immobile) configurations, depending on temperature [8,11,12]. At high temperature, the magnetic excitations induce elastic instabilities, near the temperature of the α-γ transition, which play a crucial role in the relative stability of the two types of loops. It has been shown that at low temperature $1/2\langle 111\rangle$ loops are more stable, while at high temperatures (over 700 K) ⟨100⟩ loops are more stable [13,14]. TEM observations show that in all other bcc metals, dislocation loops with a $1/2\langle 111\rangle$ Burgers vector are dominant, which suggests that they are the most stable configurations for bundles of dumbbells. Recently, much progress has been made in the experimental field, enabling observation of small ⟨100⟩ loops in W under heavy-ion irradiation at low temperatures, which vanish at high temperatures [15,16]. The reason why the ⟨100⟩ loops form in W is still under debate. In the intermediate defect cluster size range, spanning the interval between individual self-interstitial atoms and nanometric-sized dislocation loops, it is difficult to generate experimental data because of the high resolution of observations required to characterize such small objects. According to recent DFT calculations [10], SIA clusters can also form three-dimensional structures with symmetry corresponding to the C15 Laves phase. In Fe, these C15 aggregates are stable, immobile, and exhibit large antiferromagnetic moments. These C15 clusters have been found to form directly inside atomic displacement cascades, and they are able to grow by capturing self-interstitial atoms from the surrounding material.

The energetics of interstitial clusters with nanometer size plays an important role, being a key ingredient that enables the connection between the asymptotic limits: isolated point defects that can be modeled using *ab initio* methods, and large observable dislocation loops. Limitations on the size of a DFT simulation cell in transition metals does not permit the exploration of clusters containing more than a few tens of SIAs. This technical problem can be overcome in part through the development of interatomic potentials based on the embedded atom method (EAM), but then unavoidable approximations result in the loss of accuracy and transferability. Most of the EAM potentials developed to study clusters of SIAs are built to fit the energetics of small clusters of SIAs provided by *ab initio* methods [5,10,17–20]. Because of this, all the potentials provide similar results in the small cluster size limit, but there is significant scatter in the predicted formation energies over the nanometer-sized range for loops [21,22] and C15 clusters [10,23]. For instance, the EAM potentials proposed in Refs. [17–19,21,24] can be used to compute the formation energy of nanometer-sized clusters in Fe containing up to 1000 SIAs in the form of $1/2\langle 111\rangle$ dislocation loops, which span a fairly broad interval from 400 to 700 eV. Similar scatter is observed for other bcc elements, such as W, and for different types of clusters ($\langle 100\rangle$ or C15).

One way of circumventing this difficulty is to establish scaling laws from elasticity theory and then to use these laws to extrapolate DFT calculations from small clusters to larger scales. One model, proposed by Soneda *et al.* [25] two decades ago, postulated an ad hoc function for the formation energy in terms of the number n of SIAs forming the cluster. The formation energy takes the form $E_f(n) = P_0 + P_1 n^{2/3}$, where P_0 and P_1 are adjustable parameters. This popular model has been widely used in the literature. Over 100 studies have used this simple law in order to parametrize kinetic Monte Carlo or cluster dynamics simulations for the time evolution of a distribution of clusters (see, for instance, Refs. [9,26–28] and references therein). However, as we shall see later, this model yields large uncertainties at large sizes when its parameters are fitted to properties of small clusters.

In this paper, we develop a model for the energy of clusters, which combines cluster expansion and elasticity for crystalline solids, enabling us to predict the formation energies for large SIA clusters directly from *ab initio* calculations performed on small clusters. The main advantage of this model is that it successively treats the discrete nature of small clusters, combining it with the continuous nature of larger clusters such as dislocation loops. The only input required to predict the formation energies of clusters of a particular type ($\langle 100\rangle$, $1/2\langle 111\rangle$, or C15) is the formation energies of a number of configurations of small clusters of that type. To test the validity of the scaling laws derived for different types of clusters, this approach has been applied first to the case of cluster formation energies computed using EAM interatomic potentials [5,10,17–20]; after a calibration of the laws with EAM data for small clusters, we have compared the scaling law predictions for large clusters to direct computations performed using the same EAM potentials and large simulation cells. Excellent agreement was obtained for different EAM potentials and different types of clusters, which demonstrates that the subsequent calibration of the scaling laws with DFT calculations can generate formation energies for large SIA clusters with *ab initio* accuracy.

Our developments allow us to use the power of *ab initio* theory to assess the relative stability of dislocation loops with $\langle 100\rangle$ and $1/2\langle 111\rangle$ Burgers vectors and the recently proposed C15 clusters.

The paper is organized as follows. Section II describes the key aspects of the energetic model adapted to dislocation loops (Sec. II A) and to the C15 clusters (Sec. II B). The discrete-continuum model is parametrized using a database described in Sec. III A. The analysis given in Sec. III B addresses the transferability of the model. The analysis of the relative stability of SIA clusters is presented in Sec. III C. *Ab initio* scaling laws having a simple analytical form for the formation energy of self-interstitial clusters as a function of their size are presented in Sec. III D. A final discussion and conclusions are given in Sec. IV.

II. DISCRETE-CONTINUUM MODEL

A. Discrete-continuum model for dislocation loops

According to the elastic theory of dislocations [29], the formation energy of a 2D platelike cluster of SIAs is related essentially to two quantities: the line energy density of the edge dislocation, which encloses the cluster, and the stacking fault energy. The latter is very high in bcc metals, and as a result stacking faults do not form and are hence neglected in the following. The elastic energy associated with the volume V, which contains one dislocation loop bordering a cluster of n SIAs with Burgers vector $\vec{b}$, can be written using the elastic tensor C_{ijkl} and the elastic field around the loop u_i (summation over indices i,j,k,l is performed over x, y, and z) [30] as

$$E_{\text{elastic}}(n,\vec{b}) = \frac{1}{2}\sum_{i,j,k,l}\int_V C_{ijkl}\frac{\partial u_i}{\partial x_j}\frac{\partial u_k}{\partial x_l}dV. \qquad (1)$$

Using anisotropic elasticity theory and the Gauss theorem to transform the volume integral into a surface integral [13,30,31], we find the elastic contribution to the formation energy as the sum of the energy stored in the elastic field and the core energy of the edge dislocation that encloses the cluster as

$$E_{\text{elastic}}(n,\vec{b};\delta,\tilde{R},E_{c-\delta}) = \left[\oint K(\vec{t})d\vec{t}\right]\ln(\tilde{R}/\delta) + \oint E_{\delta-c}(\vec{t})d\vec{t}, \qquad (2)$$

where δ is the radius of the nonlinear dislocation core, $\tilde{R}$ is a measure of the effective range of the elastic field of the loop, and $K(\vec{t})$ is the prelogarithmic energy factor for a straight dislocation with orientation $\vec{t}$ in the bcc matrix. In the last term in Eq. (2), $E_{\delta-c}(\vec{t})$ includes the core-traction and nonlinear core energies per unit length of a dislocation. The usual assumption on $E_{\delta-c}(\vec{t})$ is to neglect the dependency on the orientation of the dislocation. If we define an average prelogarithmic factor for a circular loop as $K_a = \frac{1}{2\pi}\oint K(\vec{t})d\theta$, then the elastic energy becomes

$$E_{\text{elastic}}(n,\vec{b};\delta,E_{c-\delta}) = 2\pi R^* K_a \ln\left(\frac{R^*}{\delta}\right) + 2\pi R^* E_{\delta-c}, \qquad (3)$$

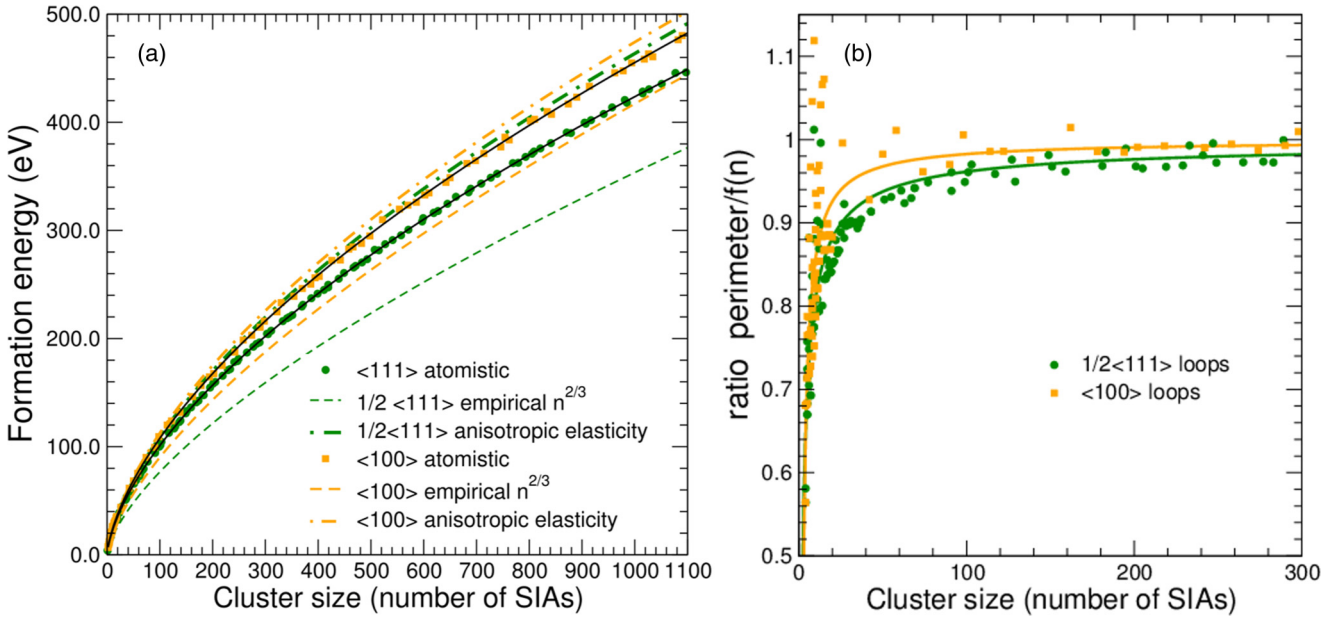

FIG. 1. (a) Formation energies of the $1/2\langle 111\rangle$ and $\langle 100\rangle$ dislocation loops in Fe against the number of SIAs, computed (i) from atomic-scale simulations using an EAM interatomic potential [18]; (ii) using predictions based on the law $P_0 + P_1 n^{2/3}$ (see Ref. [25]); (iii) using the anisotropic elasticity theory [see Eq. (5)], which is parametrized with atomic-scale calculations up to $n = 21$ SIAs. P_0 and P_1 are fitted while term T is computed directly from the elastic tensor associated with the EAM potential. (b) The ratio of the convex hull perimeter of the dislocation loops to the perimeter deduced from the discrete number n of SIAs contained in the cluster. The full curve was fitted using the function $\{1 - [1/(x^{a_1} + a_2)]\}$, with values of 0.70 and 0.88 for the exponent a_1 of $1/2\langle 111\rangle$ and $\langle 100\rangle$ loops, respectively.

where R^* is the radius of an equivalent circular loop with the same perimeter, and K_a depends also on the Burgers vector $\vec{b}$ and the habit plane. Parameter K_a is evaluated from the elastic tensor of the material C_{ijkl} using Bacon's theory [13,32,33] or Stroh's sextic formalism [30,31,34–38]. In this study, both theories have been tested and yielded very similar results. R^* is uniquely determined by the number n of SIAs. Imposing that the surface area of the loop is equal to n times the average surface area per SIA, we obtain that R^* is $f_{\vec{b}} a_{\rm bcc}\sqrt{n}$, where $a_{\rm bcc}$ is the lattice parameter of the bcc structure and $f_{\vec{b}}$ is a factor that depends on the Burgers vector and the habit plane of the loop, i.e., $f_{\vec{b}} = \sqrt{1/(2\pi)}$ and $\sqrt{\sqrt{2}/(2\pi)}$ for the $\langle 100\rangle\{001\}$ and $1/2\langle 111\rangle\{110\}$ loops, respectively. The latter consideration allows us to rewrite Eq. (3) as follows:

$$E_{\rm elastic}(n,\vec{b};\delta,E_{c-\delta}) = 2\pi\, f_{\vec{b}} a_{\rm bcc} K_a \sqrt{n} \ln\left(\frac{f_{\vec{b}} a_{\rm bcc}\sqrt{n}}{\delta}\right) + 2\pi\, f_{\vec{b}} a_{\rm bcc}\sqrt{n} E_{\delta-c}. \quad (4)$$

The elastic theory, detailed above, is adapted to the treatment of large clusters. However, we note from Eq. (4) that the elastic energy varies as the square root of n, so that for small clusters, different contributions, either from the shape of the loops or from the internal structure of the loop, are expected to become dominant below a certain value of n. Additionally, the values of δ and $E_{\delta-c}$ cannot be determined solely from elastic theory, but they must be determined from atomistic calculations. To illustrate that, we write the elastic term as a function of three unknown parameters: T, P_0, and P_1:

$$E_{\rm elastic}(n,\vec{b};\delta,E_{c-\delta}) = T\sqrt{n}\ln(n) + P_1\sqrt{n} + P_0, \quad (5)$$

where the P_0 term is introduced to match the atomic data in the limit of small SIA cluster size, e.g., $n = 1$ or 2, for which the concepts of perimeter and surface are not well defined. Using the sextic formalism [13,32], for the case of pure prismatic loop, the term T can be written as

$$T = \frac{1}{2} f_{\vec{b}} a_{\rm bcc} \ln\left(\frac{f_{\vec{b}} a_{\rm bcc}}{\delta}\right) \oint b_i b_m n_j n_q c_{ijkl} c_{npmq} \times {\rm Im}\left[\sum_{\kappa=1}^{3} \kappa_p^\eta \kappa_l^\eta \frac{N_{kn}(\kappa^\eta)}{n_s \frac{\partial D(\kappa^\eta)}{\partial \kappa_s}}\right] d\theta. \quad (6)$$

For an edge dislocation, $\vec{\kappa}^\eta = \vec{m} + \vec{n}\omega^{(\eta)}$, $\vec{n} = \vec{b}/b$, and $\vec{m} = \vec{n} \times \vec{t}$. $\omega^{(1)}$, $\omega^{(2)}$, and $\omega^{(3)}$ are the three complex roots of the sextic equation $S(\omega) = \det[c_{ijkl}(m_j + n_j\omega) \times (m_l + n_l\omega)] = 0$, which are situated in the upper half of the complex plane $\omega = {\rm Re}\omega + i\,{\rm Im}\omega$, where ${\rm Im}\omega > 0$, and $N_{ik}(\vec{\kappa})$ is the matrix adjoint to $L_{ik}(\vec{\kappa}) = c_{ijkl}\kappa_j\kappa_l$ and $D(\vec{\kappa}) = \det L_{ik}(\vec{\kappa})$. An example of parametrization of Eq. (5) is shown in Fig. 1(a). The best set of parameters for this model has been obtained using a database of clusters smaller than 22 SIAs, which are accessible to a DFT computation. The atomistic formation energies are computed using an EAM interatomic potential [18] in order to check the validity of our parametrization for large SIA clusters through a comparison between predictions and direct atomic-scale simulations. Two strategies have been tested for fitting. In the first case, all three parameters, P_0, P_1, and T were fitted. For that case, not described here, the predictions made from Eq. (5) for large clusters stringently diverge from the atomistic values, with some relative errors up to 60% for the two families of loops that have been examined. In a second method, T was

computed from the elastic tensor as shown in Eq. (6), and only P_0 and P_1 were adjusted with respect to the formation energies computed at the atomic scale for clusters with $n < 22$. Using this approach, as can be seen in Fig. 1(a), the predictions are much better since the error is around 10% for the $1/2\langle 111\rangle$ and less than 4% for the $\langle 100\rangle$ loops. The error is smaller than ad hoc laws proposed by Soneda [25] but still important in absolute terms for $1/2\langle 111\rangle$ loops. Even worse, the accuracy of the elastic model depends strongly on the choice of the database used for the fit. For the same number of clusters involved in the database, we can arbitrarily change the error by choosing various shapes of clusters. To reduce the variability of the results due to differences in the shapes of small clusters included in the database, and to reduce the relative error below 3% for the two types of loops, we must increase the maximum size of the loops included in the database to 53 SIAs. However, this is not accessible to DFT simulations in transition metals with conventional computers because to obtain the formation energies for clusters larger than 53 SIAs with reasonable accuracy, the total number of atoms needed in the simulation cell is larger than 5000. The fact that a pure elastic model parametrized on small clusters fails to correctly predict the formation energies for large clusters can be ascribed to the following two reasons: (i) the description of dislocation loops with finite core extensions is inappropriate for small clusters where the enclosing dislocation core is comparable in size to the radius of the cluster; (ii) the perimeter of the enclosing loops is fixed by a function indexed on integer values, i.e., the number of interstitial atoms. To emphasize the latter point, we have reported in Fig. 1(b) the ratio of the convex hull perimeter of loops to the perimeter deduced from n using the criterion described above. This ratio converges very slowly to 1, and for sizes included in the fit (n between 3 and 21 SIAs) the value ranges from 0.56 to 0.85. Even if the ratio of convex hull perimeter and perimeter deduced as a function of n using the $\sqrt{n}$ criterion can be improved, the ambiguity in the definition of the perimeter of small and large loops remains. Therefore, the two points noted above imply that the parameters fitted to the data derived for small loop sizes are not representative of larger loop sizes generating large errors in the adjustment/extrapolation procedure.

Hence, due to the size limitation of *ab initio* calculations, it is impossible at present—or in the near future—to parametrize an elastic model using Eq. (5) for the formation energies of SIA nanometric clusters. To overcome this difficulty, we add a cluster-expansion-like term to the elastic model, which takes into account the discrete structure of small dislocation loops:

$$E_{\text{formation}}(n) = E_{\text{discrete}}(n,n_1,n_2,\ldots;\{P_j\}) + E_{\text{elastic}}(n,b;\delta,E_{c-\delta}). \quad (7)$$

The discrete term depends on a set of parameters $\{P_j\}$, and we impose a requirement that it vanishes in the asymptotic limit $n \longrightarrow \infty$, i.e., $E_{\text{discrete}}(n,n_1,n_2,\ldots;\{P\}_j) \xrightarrow[n\to\infty]{} 0$. The discrete nature and the geometric structure of clusters are accounted for in the term E_{discrete} through a topological mapping to the local neighborhood of each dumbbell, which is defined by the number of first (n_1), second (n_2), or higher nearest-neighbor pairs of dumbbells. The distance between dumbbells is defined as the distance between their centers. For example, in the case of a $1/2\langle 111\rangle$ dislocation loop with a $\{110\}$ habit plane, the first- and second-nearest-neighbor shells each have four nearest-neighboring dumbbells, situated at distances $\sqrt{3}a_{\text{bcc}}/2$ and a_{bcc}, respectively.

The discrete part of the energy for a dislocation loop containing n SIAs is written as the sum of contributions from all dumbbells:

$$E_{\text{discrete}} = \sum_{i=1}^{n} E_i = \sum_{i=1}^{n} f\left(n;n_1^i,n_2^i\right)E\left(n_1^i,n_2^i\right). \quad (8)$$

The local energy associated with the ith dumbbell of the cluster is expressed as $E_i = f(n;n_1^i,n_2^i)E(n_1^i,n_2^i)$, where the function $E(n_1^i,n_2^i)$ fully determines how E_i depends on the dumbbell neighborhood, i.e., on the number of first- and second-nearest-neighbor dumbbells in the habit plane, denoted n_1^i and n_2^i, respectively. Function $f(n;n_1^i,n_2^i)$ fixes the weight for the ith dumbbell energy $E(n_1^i,n_2^i)$. To define the latter function, we note that various atomic-scale studies [21,39,40] have confirmed that the interatomic distance between two atoms that form the dumbbells situated far from the cluster's edges recovers bulk coordination. For example, relaxation of dumbbells recovers perfect bulk first-nearest-neighbor distance $\sqrt{3}a_{\text{bcc}}/2$ in the center of clusters. As a result, the dumbbells that are close to the center of the loops, with full nearest-neighbor shells, make no contribution to the energy of the system other than twice the cohesive bulk energy. This means that in terms of the formation energy, these dumbbells make no contribution to the discrete energy. Therefore, the function $f(n,n_1^i,n_2^i)$ should be zero for the dumbbells with their full nearest-neighbor shell. A second constraint on this function is given by the asymptotic limit at large n, i.e., $f(n;n_1,n_2) \xrightarrow[n\to\infty]{} 0$. Hence we consider the following product form: $f(n;n_1,n_2) = g(n)h(n_1,n_2)$, where $h(n_1,n_2)$ equals unity for the atoms that do not have full nearest neighborhood, and zero otherwise, and $g(n) \longrightarrow 0$ for large clusters. To ensure the condition $E_{\text{discrete}}(n,n_1,n_2,\ldots;\{P\}_j) \xrightarrow[n\to\infty]{} 0$, we have tried many monotonically decreasing functions of the form proportional to $1/n^{\alpha}$ for $g(n)$, with α in the interval from 0.5 to 1. The best choice for α was found to be 0.55.

To reduce the sum in Eq. (8), we can rewrite the discrete energy contribution by introducing the number of dumbbells having n_1 and n_2 first and second neighbors, (i_{n_1,n_2}):

$$E_{\text{discrete}} = \sum_{n_1=0}^{N_1^b}\sum_{n_2=0}^{N_2^b} i_{n_1,n_2} f(n;n_1,n_2)E(n_1,n_2) + P_2, \quad (9)$$

where N_1^b and N_2^b are the bulk numbers of first and second neighbors, and P_2 is a constant. A pair formulation is neither a necessity nor a constraint in this approach, since the model can be readily extended to more complex types of interaction. To exemplify this energetic model, let us take the example of a small $\langle 100\rangle\{001\}$ loop containing 15 SIAs, which is sketched in Fig. 2. In this case, the discrete part of the energy can be written as

$$E_{\text{discrete}} = \frac{1}{15^{0.55}}[2E(1,2) + 4E(2,2) + 3E(2,3) + 2E(4,2) + 3E(4,3)] + P_2. \quad (10)$$

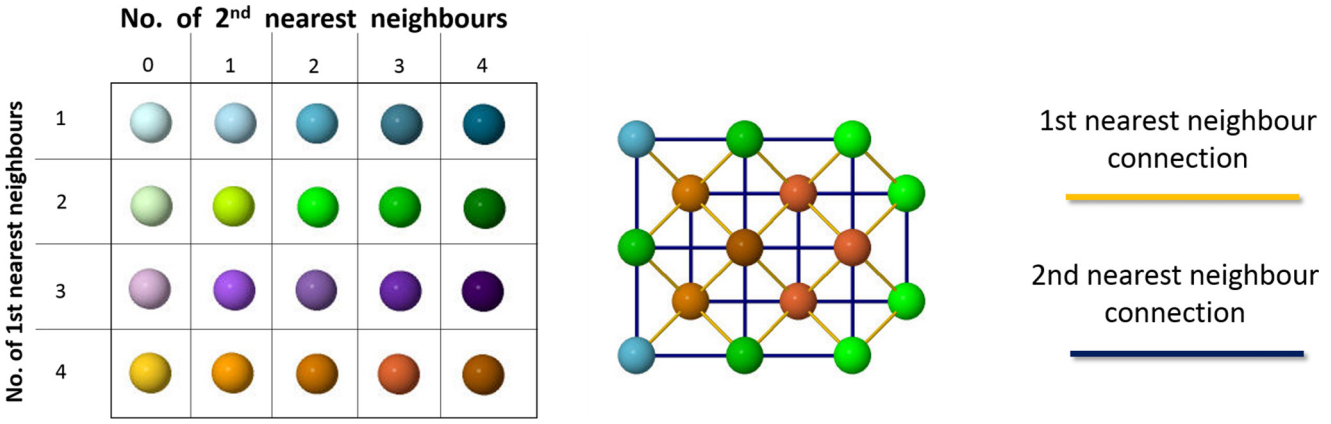

FIG. 2. Structure of a ⟨100⟩ loop in the {001} habit plane containing 15 SIAs showing the number of first and second nearest neighbors of all dumbbells. Note: The loops were constructed such that each dumbbell has at least one dumbbell in the first-nearest-neighbor position. As a result, the possible number of first nearest neighbors varies from 1 to 4, while the number of second nearest neighbors varies from 0 to 4. There exists just one exception, namely the case of mono-SIA.

In the above equation, $h(4,4) = 0$ and $h(1,2) = h(2,2) = h(2,3) = h(4,2) = 1$.

Combining the elastic and discrete parts, we find that the formation energy of a loop with n SIAs is

$$E_{\text{formation}}(n) = T\sqrt{n}\ln(n) + P_1\sqrt{n} + P_0 + \sum_{n_1=0}^{N_1^b}\sum_{n_2=0}^{N_2^b} i_{n_1,n_2} \times f(n;n_1,n_2)E(n_1,n_2). \quad (11)$$

We note that parameter P_0 derived from elasticity is combined with P_2, deduced from the discrete model, to give just one constant, denoted by P_0 in Eq. (11). Our goal here is to produce an analytical model that defines a general functional form of the scaling law that describes the formation energy $E_{\text{formation}}(n)$ of clusters as a function of their size n. The advantage of this formulation, expressed in Eq. (11), is that a full set of parameters $E(n_1,n_2)$ and $P_{0,1}$ can be obtained from *ab initio* formation energies derived using a training series of configurations of small interstitial clusters. The model combines a discrete contribution to the energy, evaluated using a cluster expansion formalism, with a term derived using a treatment of prismatic loops based on elasticity theory. The predicted formation-energy values are going to be used to determine the functional form of the energy scaling law, as described in Sec. III.

B. Discrete-continuum model for C15 clusters

The strategy described above has also been adopted to develop a model for C15 clusters. C15 inclusions have different elastic properties in comparison to the host bcc matrix [41], and the corresponding energy is treated using the formalism of isotropic Eshelby inclusion [30,42,43]. The discrete contribution to the formation energy takes into account the particular structure of C15 clusters. In comparison with the case of dislocation loops, they have an additional contribution from the atoms having perfect C15 bulk coordination situated inside the clusters. Thence the core region of a C15 cluster does contribute non-negligibly to the formation energy. In addition, the bcc bulk atoms of the perfect lattice are replaced by C15 bulk atoms with different cohesive energies, and consequently this difference must be accounted for. The remaining atoms of the SIA cluster, which do not have the perfect C15 bulk coordination, correspond to the interface between the C15 cluster and the bcc matrix. These interfacial atoms also contribute significantly to the formation energy. The present energetic model is close to the Zhang *et al.* [23] model used for interpolating the formation energy of C15 clusters provided by EAM interatomic potential calculations. In the model of Zhang *et al.*, the number of atoms situated both at the interface and in the perfect C15 bulk is deduced from the asymptotic limit of large clusters. The present model is used for predicting the formation energy of C15 clusters from DFT calculations. The difference between the convex hull surface and the surface computed from the number of SIAs in a cluster is fairly large for small sizes [even larger than that for the perimeter of loops, Fig. 1(b)]. Therefore, the number of atoms with perfect C15 bulk coordination N_{C15}, the number of interfacial atoms N_i, as well as the surface area S_{C15} and volume V_{C15} of C15 clusters are deduced directly from the geometry of the cluster. The formation energy expression used in our model is written as follows:

$$E_{\text{formation}}(n) = S_{\text{C15}}\gamma + \frac{6V_{\text{C15}}\mu\varepsilon^2}{\alpha} + N_{\text{C15}}\left(E_{\text{coh}}^{\text{bcc}} - E_{\text{coh}}^{\text{C15}}\right) + N_{\text{i}}\Delta E_{\text{i}}, \quad (12)$$

where $E_{\text{coh}}^{\text{bcc}}$ and $E_{\text{coh}}^{\text{C15}}$ are the cohesive energies of the perfect bulk bcc and of the perfect C15 structures, respectively. The coefficient ΔE_i is the average energy of atoms at the interface, and γ is the interface energy per unit area between the bcc matrix and the C15 inclusion. The second term in Eq. (12) is the energy of isotropic Eshelby's inclusion, with a C15 cluster treated as an inclusion in the otherwise isotropic bcc matrix. Eshelby discovered an elegant way of calculating the stress, strain, and displacement fields, both in the inclusion as well as in the matrix, by using a superposition of linear elasticity and the Green's-function formalism [42,43]. The same approach allows the computation of the strain energy contribution in the presence of a C15 cluster. Here, μ is the isotropic shear modulus of the matrix, while $\alpha = 1 + 3\mu/(4B_{\text{C15}})$, where

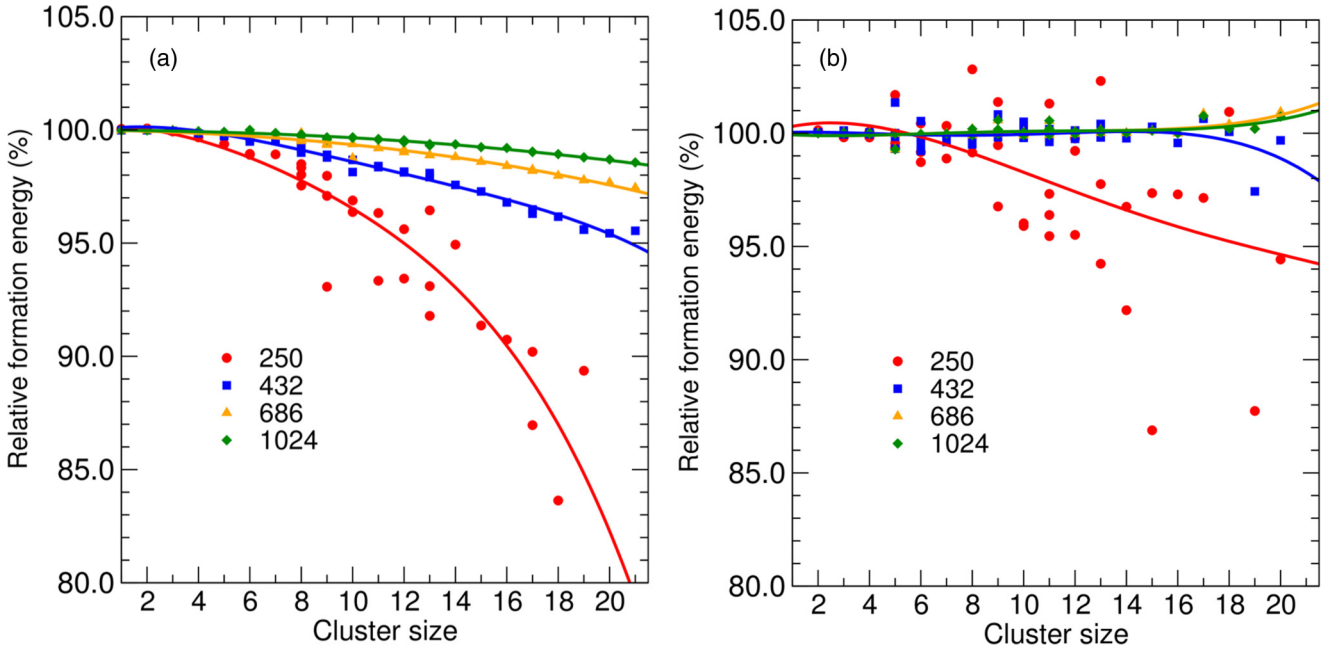

FIG. 3. Formation energies of n SIAs of (a) $1/2\langle 111\rangle$ and (b) $\langle 100\rangle$ dislocation loops in Fe, computed with an EAM potential [18] with different configurations in cubic simulation cells containing $250+n$ (red circle), $432+n$ (blue square), $686+n$ (orange triangle up), and $1024+n$ (green rhombus) atoms. All energies are normalized to the asymptotic limit, taken as the formation energy in a simulation cell containing $207\,646+n$ atoms. Lines are guides for the eyes, obtained using a fit to a fourth-order polynomial. Formation energies have been corrected using the elastic dipole correction method to account for the finite size of the simulation cells [47].

B_{C15} is the bulk modulus of C15 clusters and ε is the misfit strain, which can be computed directly from atomic-scale calculations. ΔE_i and γ are adjusted with respect to atomic-scale simulations, while the cohesive energies of bcc and C15 clusters are determined from atomistic calculations [41]. In the limit of large spherical C15 clusters, the previous equation can be written as a function of the number n of SIAs as in the Zhang model [23]:

$$E_{\mathrm{formation}}(n) = 2\gamma_s(9\pi\Omega^2)^{1/3}n^{2/3} + \frac{12\Omega\mu\varepsilon^2}{\alpha}n + 3n\left(E_{\mathrm{coh}}^{\mathrm{bcc}} - E_{\mathrm{coh}}^{\mathrm{C15}}\right), \quad (13)$$

where Ω is the atomic volume of bcc iron. In the large limit, a cluster with n interstitials is obtained by replacing $2n$ bcc atoms by $3n$ C15 atoms, which gives the volume of the C15 cluster as $V_{\mathrm{C15}} = 2n\Omega$. The convex hull surface and the atomic interface energies, i.e., the first and last terms of Eq. (12), have been combined into a single term that is the first term of Eq. (13). The prefactor γ_s in the first term, which gives the dependence in $n^{2/3}$, plays the role of interface energy. Due to the fact that the S_{C15} and N_i terms of the discrete formulation in Eq. (13) take the form $n^{2/3}$ in the infinite limit, the interface energy γ_s combines γ and ΔE_i.

III. PARAMETRIZATION AND RESULTS

A. Database used for parametrization of the discrete-continuum model

The energy landscape of dislocation loops has been widely studied at the atomic scale by various authors [13,21,33,44,45], and the lowest-energy configurations of various clusters have already been reported in the literature. $1/2\langle 111\rangle$ dislocation loops were generated by inserting $\langle 111\rangle$ dumbbells in the $\{110\}$ habit plane so as to form compact clusters. $\langle 100\rangle$ dislocation loops were generated by inserting atomic $\langle 100\rangle$ dumbbells in the $\{001\}$ habit planes. In addition to these configurations, we have found that some specific cluster geometries needed to be included in the database in order to have a good parametrization for $E(n_1,n_2)$. The choice of these configurations was made to reproduce the neighborhood of large loops, i.e., those containing thousands of SIAs (see the Appendix A for further details). In this work, the size of the clusters included in the database is limited by the feasibility of *ab initio* calculations. The size of the clusters in the database ranges from 2 to 20 SIAs with a total of about 50 configurations for $\langle 100\rangle$, and from 2 to 22 SIAs with 31 configurations for $1/2\langle 111\rangle$. The choice of the largest cluster size, i.e., 22 SIAs for $1/2\langle 111\rangle$, is justified by the low relative error in the formation energy in simulation cells with $1024+n$ atoms ($8a\times 8a\times 8a$ cells). As shown in Fig. 3, the relative errors in the formation energies due to this size limit are lower than 2%. More details, along with the exhaustive list of configurations included in the database, are given in the Appendix A.

The building block of C15 clusters is a di-interstitial cluster. A simple way to insert a di-interstitial C15 cluster into a bcc matrix is to place a Z16 Frank-Kasper polyhedron having 12 atoms at the interstitial positions [see Fig. 4(a)] together with 10 vacancies around a given bcc atomic site. Larger C15 clusters can be described as sums of Z16 Frank-Kasper polyhedra having centers situated on a diamond network, which underlies the initial bcc structure [this network is shown

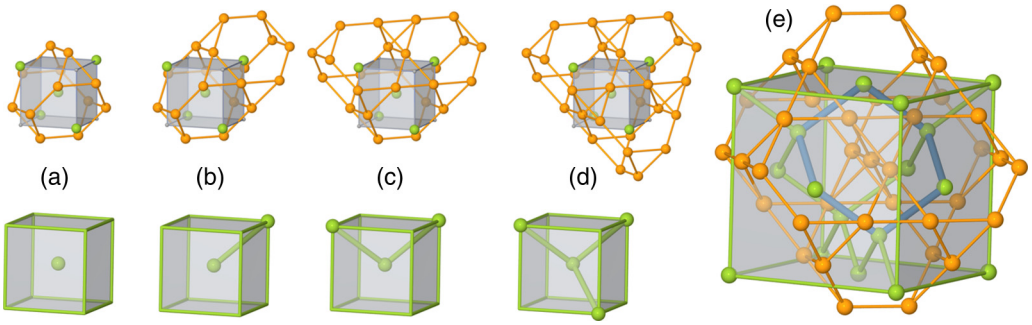

FIG. 4. (a)–(d) Top: Structure of small C15 interstitial clusters in a bcc lattice of the di-, tetra-, hexa-, and octo-interstitial clusters, in a skeleton representation, i.e., only SIAs are represented as orange spheres without any representation of vacancies and cubic lattice sites. (a)–(d) Bottom: centers of the Z16 Frank-Kasper polyhedron corresponding to the top C15 skeletons are represented by green spheres. (e) The 11 SIA C15 cluster, the lowest size that forms a closed ring with the centers of Z16 Frank-Kaspers polyhedra. This ring is emphasized by blue bonds connecting the centers of Z16 polyhedra.

in Figs. 4(a)–4(e)]. The present database should include the lowest-energy configurations. To form a cluster with a given number of SIAs, the number of possible choices of Z16 centers is quite large, and guessing the configurations with the lowest formation energies is problematic. The database for C15 clusters contains up to 20 configurations of SIAs. This limit is fixed, as in the case of loops, by the accuracy in the formation energies derived from DFT calculations with a cell containing $1024 + n$ atoms. Systematic exploration of the energy landscape in search of the minimum energy C15 configurations gives good results for small clusters. Marinica *et al.* [10] used the activation relaxation technique [46] for finding the lowest-energy configurations for two, three, or four SIA clusters. Nonetheless, the number of possible configurations grows exponentially with the size of the cluster, making a systematic search prohibitive at larger sizes. More advanced techniques using a genetic algorithm were proposed, making it possible to find the lowest-energy configurations containing up to 10 SIAs [48]. In a more pragmatic approach, configurations for the present database were generated using three "selection rules" that have been established from the observation of the formation energies of several trial configurations generated using EAM potentials [18,21,24]:

(i) All Z16 centers must be connected by at least one nearest-neighbor bond to another center. This rule prevents the construction of configurations formed by disconnected clusters.

(ii) Closed hexagonal paths made of six Z16 centers are favored whenever possible. The smallest cluster having six Z16 connected centers is the 11 SIA cluster, which is shown in Fig. 4(e). Loop closure then occurs for specific sizes, referred to as magic numbers. The next magic numbers are observed for 17 and 23 SIAs. These structures indeed have very low formation energies. The next step is to eliminate different possible constructions containing the same numbers of SIAs. Careful observation reveals that closed loops in compact form have lower formation energies if compared to closed loops in planar form.

(iii) The C15 clusters must be constructed in the most compact 3D way.

The C15 configurations for validation data were also generated using these three rules.

B. Validation of the discrete-continuum model using different EAM potentials

The discrete-continuum model can be parameterized through simulations performed using different EAM interatomic potentials, which allows us to test model predictions for large clusters, using large simulations cells. Several EAM potentials for Fe [17,18,21,24] and for W [5,20,49,50] were used for our tests. Note that in the Fe EAM potential published in Ref. [21], a typo was corrected in Ref. [10].

The set of cluster geometries used for training the discrete-continuum model with EAM energies is the same as the one that will be used later for parametrizing the model from DFT data. The tests were performed for $\langle 100\rangle\{100\}$ and $1/2\langle 111\rangle\{110\}$ dislocation loops containing up to 1200 SIAs. Three types of shapes were considered to construct configurations: rectangular, circular, and hexagonal, where the sides of the polygon correspond to the dense directions of the habit planes. The database of C15 clusters contains configurations with sizes up to 110 SIAs. The C15 configurations were mostly generated in accordance with the three rules mentioned in the previous section. The few configurations that do not obey these rules will be discussed later.

The atomistic formation energies of clusters of SIAs were computed using zero Kelvin atomic relaxation simulations. The asymptotic values of the formation energies were obtained by introducing interstitial clusters in a constant volume simulation cell with millions of atoms, sufficient to remove any residual size effect. The system was relaxed using a conjugate gradient technique with a convergence criterion on the maximal force per atom of lower than 0.02 eV/Å. We have also performed calculations where the criterion was 0.001 eV/Å, resulting in minor changes in the formation energies, less than 0.001 eV.

The formation energies calculated with EAM potentials were compared with predictions made using the discrete-continuum model (see Fig. 5). For dislocation loops, the difference is less than 2% [see Figs. 5(a) and 5(b) for $1/2\langle 111\rangle$ and $\langle 100\rangle$ loops, respectively] using the EAM potential from Ackland-Mendelev for Fe [18]. Similar results are obtained for all the EAM potentials tested for Fe and W. For the C15 clusters, the error is slightly larger, i.e., 3% [see Fig. 5(c)]. The error may reach 5% for some clusters, e.g., clusters containing

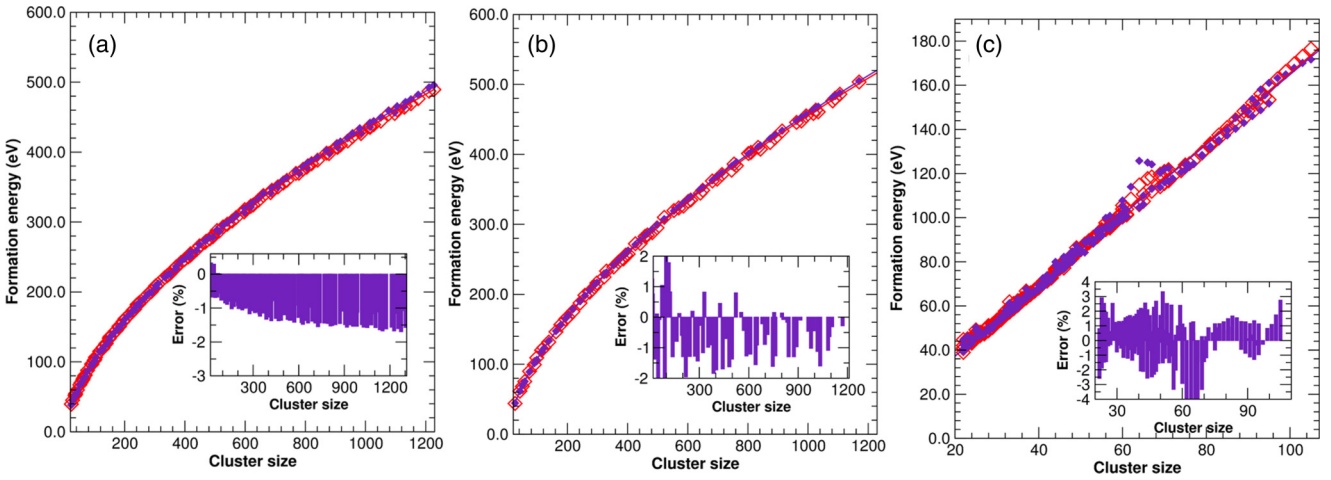

FIG. 5. Cluster formation energies as a function of cluster size for (a) $1/2\langle 111\rangle$ and (b) $\langle 100\rangle$ loops and for (c) C15 SIA clusters in Fe calculated using the Ackland-Mendelev potential for Fe [18]. Open diamonds represent the direct EAM results derived from simulations using large cells, while blue full diamonds represent values predicted by the discrete-continuum model. The relative errors are plotted as insets. Note that for the nanometric clusters, the relative error is less than 3%.

62, 64, 66, and 67 SIAs. The main reason for this discrepancy is that such clusters do not have compact geometries, hence they break the spherical symmetry assumed in the model. These configurations were created by infringing the third rule given in Sec. III A. We estimate that such configurations are not significant for the purpose of this study, being far from the lowest-energy configurations.

C. *Ab initio* based predictions of SIA cluster formation energies

Having validated the discrete-continuum model, we can now proceed to its parametrization using the DFT formation energies of configurations included in our database. The DFT simulation cell for n SIAs has been chosen to contain between $250+n$ and $1024+n$ atoms in such a way that the relative error in the formation energy is lower than 2% from the converged values (see Fig. 3). The DFT calculations were performed using VASP within the projector augmented wave (PAW) framework [51]. The plane-wave energy cutoff is 350 eV and the Hermite-Gaussian broadening width for Brillouin zone integration is 0.2 eV. The calculations are performed including the p semicore states. The exchange correlation energy is evaluated using the Perdew-Burke-Ernzerhof (PBE) generalized gradient approximation (GGA). The k-point grid mesh was chosen from 3^3 for the $250+n$ cell up to (1 or 2^3) for the $1024+n$ cell. W and V are nonmagnetic materials, and iron is treated in the ferromagnetic state, which is a reasonable approximation in the low-temperature limit. Each configuration is relaxed using the conjugate gradient technique with a convergence criterion on the force on each atom of 0.02 eV/Å. The size of the supercell remains fixed in order to ensure constant volume-per-atom simulations. All the formation energies were adjusted using the dipole correction [47]. Varvenne *et al.* [47] have proved that dipole correction from constant volume, or zero strain, yields a good correction value for the formation energy of defects in ferromagnetic iron, such as dislocation loops or C15 clusters.

The formation energies for the $\langle 100\rangle$ and $1/2\langle 111\rangle$ loops, as well as C15 clusters, were computed for Fe, W, and V (except $\langle 100\rangle$ for V), and the results are shown in Figs. 6, 7, and 8, respectively.

As mentioned earlier, for all bcc metals, the experimental evidence, within the limit of detection in TEM, for instance 1–2 nm radius for loops, confirms that the most frequently observed morphology at low temperature corresponds to $1/2\langle 111\rangle$ loops. The formation energies predicted by the discrete-continuum model for large dislocation loops (sizes larger than hundreds of SIAs) are in agreement with this observation since the $1/2\langle 111\rangle$ loops are predicted to be energetically more stable. The model also shows that, for dislocation loops from 10 SIAs to sizes visible in TEM, $1/2\langle 111\rangle$ loops always have smaller formation energy than the $\langle 100\rangle$ loops in both Fe and W. The present study is at odds with some EAM potentials for Fe [10,21] and for W [5,33,50], which predict a crossover in the relative stability of two families of loops around 200 SIAs. Below this critical size, the $\langle 100\rangle$ loops would be more stable in W whereas they would be more stable above the critical size in Fe. The origin of this inversion in the relative stability of loops is still unclear. It is worth noting that the discrete-continuum model is able to reproduce the crossover predicted by the EAM potentials if the model was calibrated using the database corresponding to the same potential. When the model is calibrated to the database derived from DFT, the model predicts no crossover between the loop formation energies.

In contrast, the DFT-based predictions show crossovers between C15 clusters and loops. In Fe, one crossover appears with $1/2\langle 111\rangle$ loops at clusters around 51 SIAs in size, corresponding to a 1.5-nm-diam C15 cluster. There is also a crossover with $\langle 100\rangle$ loops, this time both in W and Fe at 21 and 91 SIAs, respectively. In V there is no crossover; $1/2\langle 111\rangle$ loops are the most stable configurations for all defect cluster sizes.

In Fe, the present results reconcile the theoretical predictions with experiments, where only the $1/2\langle 111\rangle$ loops were observed under irradiation at low temperature, by giving some support to a mechanism recently identified as a possible route of formation of the $1/2\langle 111\rangle$ and $\langle 100\rangle$ loops involving

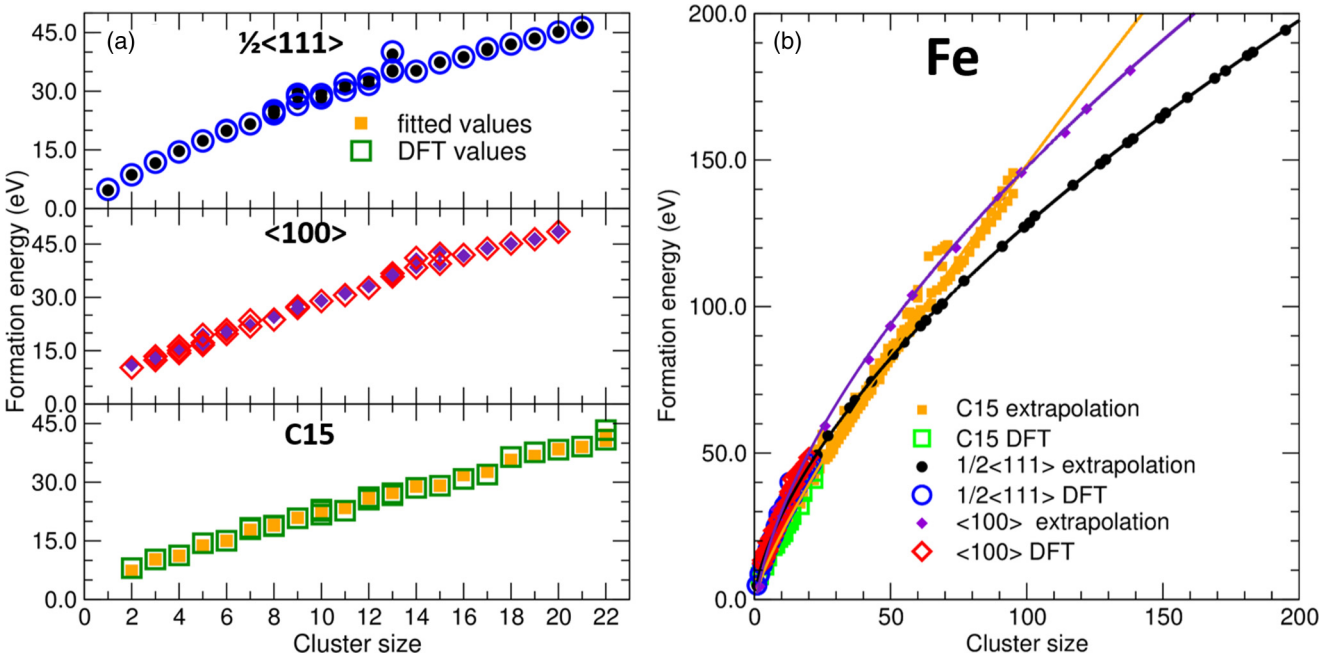

FIG. 6. (a) DFT formation energies of $1/2\langle 111\rangle$, $\langle 100\rangle$, and C15 clusters in Fe (empty circles, squares, and diamonds, respectively), and the DFT-based predictions made using the discrete-continuum model (full circles, squares, and diamonds, respectively). (b) Extrapolation of the formation energies at large sizes for the $1/2\langle 111\rangle$ loops, $\langle 100\rangle$ loops, and C15 clusters in Fe, empty symbols. Full lines represent the elastic model [Eq. (5)] parametrized using the points predicted by the present discrete-continuum model. This extrapolation can be done without size limitation. Note the crossover between $1/2\langle 111\rangle$ loops and the C15 clusters at 51 SIAs, and between $\langle 100\rangle$ loops and C15 clusters at 91 SIAs.

the collapse of larger C15 clusters [23]. The possible formation mechanisms of $\langle 100\rangle$ loops in Fe were addressed in the past in several studies, and some examples are given in Refs. [52–55]. In particular, Refs. [52–54] propose a mechanism based on the reaction between two $1/2\langle 111\rangle$ loops having appropriate size and specific orientations. The mechanisms proposed by Marian *et al.* [52] and Xu *et al.* [53] are similar, the only difference being that Xu *et al.* showed that this reaction holds

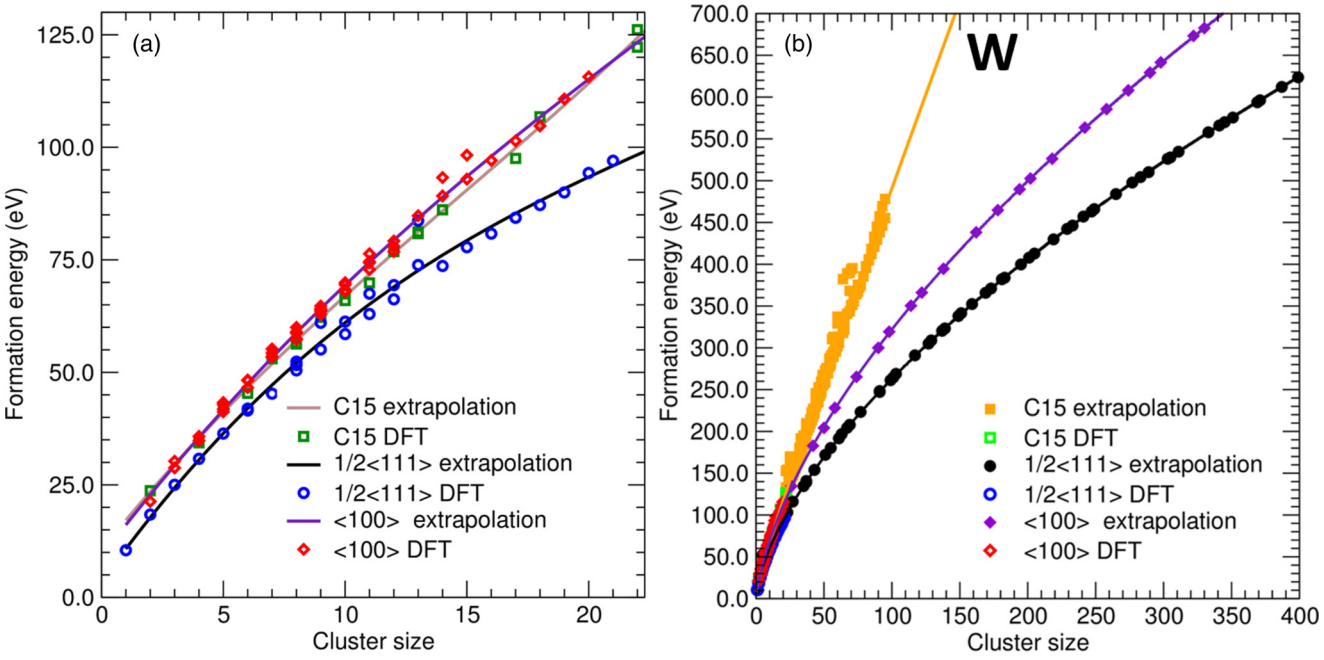

FIG. 7. (a) DFT formation energies of $1/2\langle 111\rangle$, $\langle 100\rangle$, and C15 clusters in W (empty circles, squares, and diamonds, respectively) and the DFT-based extrapolation from the discrete-continuum model (colored lines). (b) Extrapolation of formation energies at large sizes for the $1/2\langle 111\rangle$ loops, $\langle 100\rangle$ loops, and C15 clusters in W, empty symbols. Full lines represent the elastic model [Eq. (5)] parametrized on the points predicted by the present discrete-continuum model.

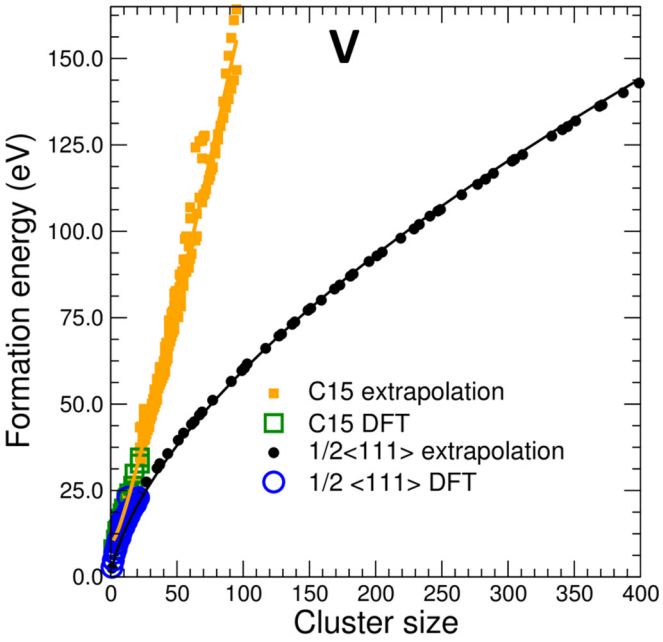

FIG. 8. DFT and discrete-continuum model predictions for the formation energies of $1/2\langle 111\rangle$ interstitial loops and C15 SIA clusters in V. The same conventions as in Figs. 6 and 7 are used.

for larger clusters and has stochastic components. Another scenario by Chen *et al.* proposed transformation of $1/2\langle 111\rangle$ loops into $\langle 100\rangle$ by correlated translation-rotation of SIAs forming the loop [55]. All of these mechanisms involve a certain number of stringent conditions, such as the direction of loop migration and the size of the loops, which make the corresponding events highly infrequent. Zhang *et al.* [23] proposed an alternative idea involving the nucleation of C15 clusters and their growth by trapping of single self-interstitials of $1/2\langle 111\rangle$ dumbbell structure. In Fe, small C15 clusters are energetically very stable and act as traps for small mobile SIAs. Moreover, they are kinetically trapped, meaning that the lowest-energy reaction pathway that allows C15 clusters to transform into planar loops corresponds to very large energy barriers resulting in highly improbable transitions. In Ref. [10], it was shown that the lowest-energy pathway that transforms a four-SIA C15 cluster into a planar loop is of the order of a few electronvolts. Under irradiation, small mobile interstitial clusters, such as $1/2\langle 111\rangle$ or $\langle 110\rangle$ loops, are continuously produced, facilitating the growth of C15 clusters, which can reach very large sizes, even larger than the crossover between C15 and traditional loops because of their kinetic trapping.

At large sizes, the transformation of C15 clusters into dislocation loops with $1/2\langle 111\rangle$ or $\langle 100\rangle$ orientation becomes very likely. This transformation was demonstrated even on the time scale of molecular-dynamics simulations by Zhang *et al.* [23]. Therefore, the frequency of formation of $\langle 100\rangle$ loops is definitely larger than in any other mechanism proposed in the past. The only condition is that the C15 clusters should be formed at small sizes, which is confirmed by DFT calculation of [10] and the present study for small (up to eight SIAs) and large clusters (nanometric sized), respectively. Although the mechanism proposed by Zhang *et al.* is rather convincing to explain the formation of $\langle 100\rangle$ loops at high temperature in Fe, it does not explain why these loops are not observed at low temperature [14]. The present work resolves this contradiction by revealing the DFT relative energy of large clusters. The interpretations of the mechanism of Zhang *et al.* were based on the EAM potential energetic landscape, which is different from the present DFT findings. As shown in Fig. 6, the crossover between the C15 clusters with $\langle 111\rangle$ and $\langle 100\rangle$ loops occurs at 51 and 91 SIAs, respectively, in Fe. This means that the C15 clusters, which could form under irradiation and have sizes larger than 51 and smaller than 91 SIAs, can decay only into the $1/2\langle 111\rangle$ clusters. This could explain the absence of $\langle 100\rangle$ loops because the C15 clusters are more stable in this size range (between 51 and 91 SIAs). We expect that C15 clusters should have sizes much larger than 91 SIAs in order to have nonzero probability to transform into $\langle 100\rangle$ loops, which further increases the size range where $\langle 100\rangle$ cannot appear. Even though our interpretation does not exclude the possibility of $\langle 100\rangle$ loop formation directly under irradiation at low temperature, it drastically reduces such a probability, in agreement with experimental observations [14,56].

For small cluster sizes in W and V, the formation energies of C15 clusters are much higher than for $1/2\langle 111\rangle$ loops. In W for small sizes, between 7 and 21 SIAs, the C15 clusters have slightly lower formation energies than $\langle 100\rangle$ loops, as shown in Fig. 7(a), and $\langle 100\rangle$ clusters become energetically more favorable than the C15 clusters containing more than 21 SIAs. In V, $\langle 100\rangle$ loops have formation energies that are between those of $1/2\langle 111\rangle$ loops and C15 clusters at all sizes. We used a relatively restricted set of calculations to parametrize an energetic model for $\langle 100\rangle$ loops in V, and so this conclusion is given on the basis of calculations for intermediate cluster sizes performed for 2, 4, 10, and 20 SIA clusters.

D. *Ab initio* scaling laws for formation energy

One of the goals of this paper is to provide a simple analytical scaling law formula for the formation energy of self-interstitial clusters. The interest of such a formulation is the practical application in multiscale techniques including kinetic Monte Carlo simulations and cluster dynamics or dislocation dynamics studies. Using the present analytical scaling law, we restrict the input required for parametrization of defect energetics to the number of interstitial atoms and their type. These new simple scaling laws provide reliable formation energies over a very broad range of defect sizes for any subsequent multiscale study.

Therefore, based on the dependence of the elastic contribution of the formation energy of loops [in Eq. (5)] and C15 clusters [in Eq. (13)] on the number of interstitials, we propose a simple analytical expression in order to fit the formation energies predicted by the discrete-continuum model, for the loops,

$$E_f(n) = a_0\sqrt{n}\ln(n) + a_1\sqrt{n} + a_2, \tag{14}$$

and of C15 clusters,

$$E_f(n) = a_0 n^{2/3} + a_1 n + a_2. \tag{15}$$

It is worth noting that for sizes larger than 15 SIAs, these two laws are a very good fit to the formation energies. In the case

TABLE I. Best-fit parameters [Eqs. (14) and Eq. (15)] for the formation energies extrapolated using the discrete-continuum model for the three types of clusters in three different bcc crystals. a_0, a_1, and a_2 are expressed in eV.

	a_0			a_1			a_2		
Element	$1/2\langle 111\rangle$	$\langle 100\rangle$	C15	$1/2\langle 111\rangle$	$\langle 100\rangle$	C15	$1/2\langle 111\rangle$	$\langle 100\rangle$	C15
Fe	1.60485	1.77677	0.453304	5.35226	7.15951	1.35469	−0.147319	−5.81801	9.35418
W	3.92996	4.84883	1.09667	7.92419	13.69844	3.32949	6.20090	−8.25849	44.68020
V	1.03029		1.53649	0.85406		1.34986	3.86213		−7.35361

of dislocation loops, the absolute error is lower than 1 eV. The parameters of Eqs. (14) and (15) for Fe, V, and W are given in Table I. For any subsequent use, it is recommended to compute the formation energies using best-fit parameters from Table I in Eqs. (14) and (15) for cluster sizes higher than $n = 15$. For lower values of n, the formation energies of various configurations are provided in Appendix B.

IV. CONCLUSIONS

In this paper, we investigated the formation energies of SIA clusters in three bcc metals, namely Fe, W, and V. The main result was the development and validation of a discrete-continuum model that makes it possible to perform *ab initio* accuracy-level calculations for clusters without any size limitation. The model allows us to treat various cases of interstitial dislocation loops and C15 clusters from clusters containing a few SIAs to nanometer size.

From the interpretation of the present results, it can be concluded that above ∼100 SIAs $1/2\langle 111\rangle$ loops are always the most stable family of SIA clusters—in agreement with experimental observations of irradiation defects at low temperature in bcc metals. However, these results are at odds with calculations made using various EAM interatomic potentials, which yield spurious predictions concerning the relative stability of $\langle 100\rangle$ and $1/2\langle 111\rangle$ loops [21]. Future developments of such potentials should consider the information provided in the present paper, and include the appropriate additional fitting conditions on the potential parameters.

Our study shows that in Fe, C15 clusters are the most stable clusters of defects for sizes lower than 51 SIAs, which is a size range not accessible to direct TEM observations. Our model also supports the theory of formation for $\langle 100\rangle$ loops proposed by Zhang *et al.* [23]. In the present work, we do not include thermal effects and magnetic excitations. As a consequence, our results are comparable only to low-temperature experiments. The results obtained shed some light on the absence of $\langle 100\rangle$ loops in low-temperature experiments, and they reconcile the Zhang mechanism with the experimental evidence. However, in order to validate entirely our expectations, further analysis is required.

Finally, our work makes it possible to establish scaling laws for the formation energies of various types of clusters in various materials, which is significant for multiscale simulations such as kinetic Monte Carlo simulations [9,27,57–59], cluster dynamics studies [60,61], or mean-field approximations [62], where simple analytic laws are needed to model the energy of large clusters. However, to enable the use of scaling laws in multiscale simulations, the effects of temperature must be accounted for. The present formulation of the discrete-continuum model can be extended to address the formation free energies, e.g., by including the temperature dependence of elastic constants.

ACKNOWLEDGMENTS

This work has been carried out within the framework of the EUROfusion Consortium and has received funding from the Euroatom research and training program 2014-2018 under Grant Agreement No. 633053. The views and opinions expressed herein do not necessarily reflect those of the European Commission. The research leading to these results was partly funded by the European Atomic Energy Community's (Euratom) Seventh Framework Programme FP7/2007-2013 under Grant Agreement No. 604862 (MatISSE project) and in the framework of the EERA (European Energy Research Alliance) Joint Programme on Nuclear Materials. R.A., F.W., and M.C.M. acknowledge the support of the French Agence Nationale de la Recherche (ANR) under project EPigRAPH ANR-14-CE07-0001. R.A. and M.C.M. acknowledge support from the GENCI -(CINES/CCRT/IDRIS) computer center under Grant No. x2016-096973 and from PRACE (Partnership for Advanced Computing in Europe) for access to the resource MareNostrumIII at the Barcelona supercomputing center (TRANSOM project). M.G. and S.D. also received funding from the RCUK Energy Programme (Grant No. EP/I501045). R.A. and M.C.M. thank E. Clouet for insightful discussions and suggestions about this work. We are also grateful to E. Clouet for giving us the opportunity to compare our results for the term T of Eq. (6) with the results provided by BABEL code [31].

APPENDIX A

Parametrization of the discrete part of the present energetic model relies on the topology of cluster configurations. The number of first or second nearest neighbors of each dumbbell is an essential ingredient for the formation energy calculations in Eq. (11). In this Appendix, we present the constraints that we have imposed in the construction of cluster geometries in order to set up correctly, from a mathematical point of view, the fitting procedure of $E(n_1,n_2)$ parameters.

The construction of the extrapolation database is based on older studies of various authors [13,21,33,44,45] that assert that closed-loop configurations, such as rectangles, squares, or circles, are more stable than possible elongated configurations for the same number of SIAs. Adhering to this requirement, hundreds of configurations of $\langle 100\rangle$ and $1/2\langle 111\rangle$

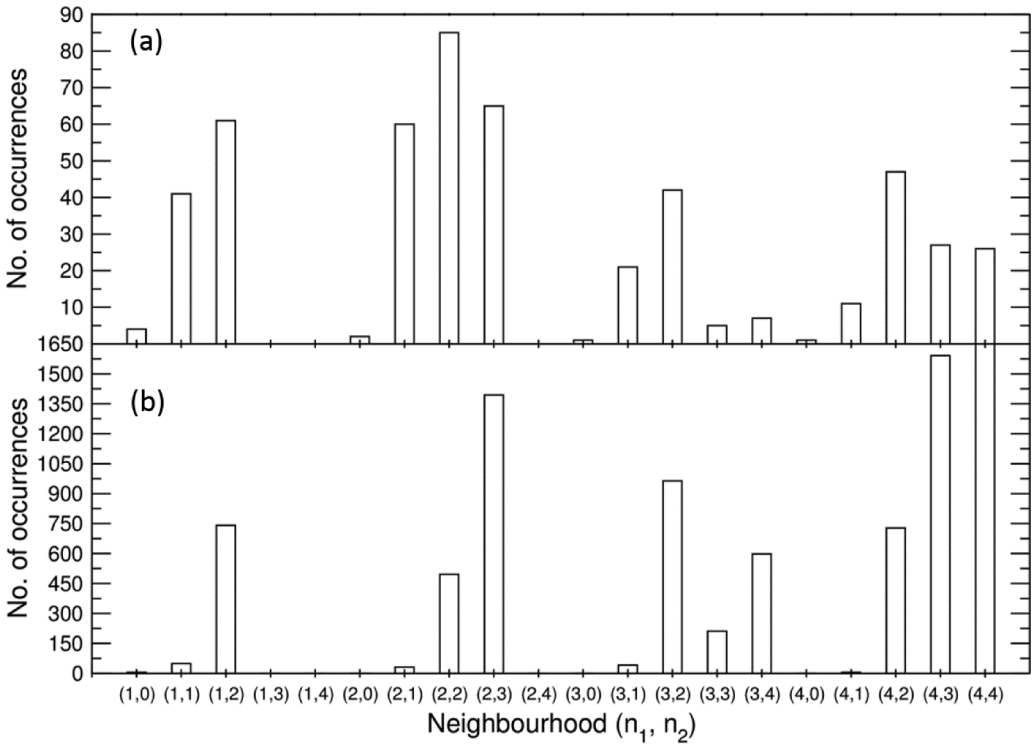

FIG. 9. Histograms showing the number of occurrence of pairs of dumbbells with respect to the type (n_1,n_2) for all (a) training (small clusters) and (b) validation (small up to large clusters) ⟨100⟩ configurations, where n_1 is the number of first nearest neighbors and n_2 refers to the number of second nearest neighbors. Possible (n_1,n_2) dumbbell pairs of the type $(0,n)$, where $n = 0$–4 were not included due to absence of such pairs in both training and validation configuration sets.

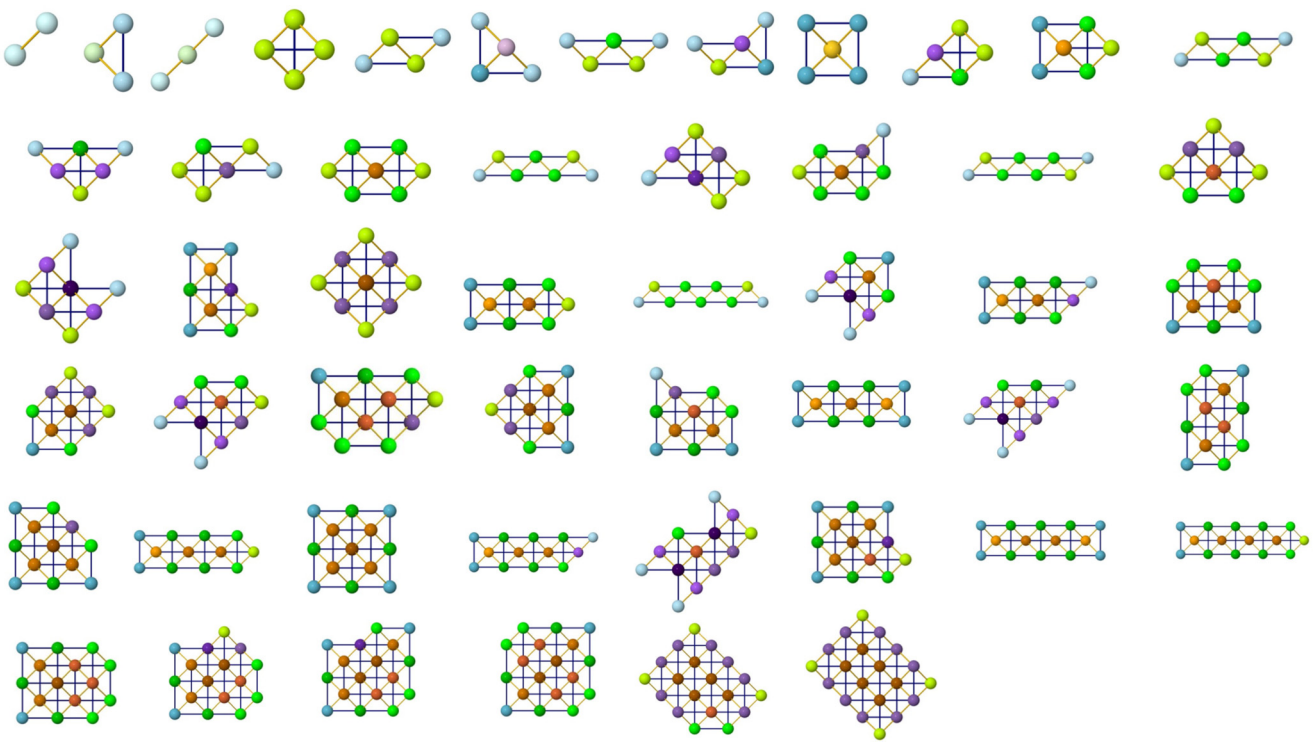

FIG. 10. Database configurations of ⟨100⟩ loop type. The cluster dumbbells are projected (and represented) in the {001} habit plane. The color of each dumbbell is assigned according to the number of first and second neighbors, (n_1,n_2). The color assignment map is shown in Fig. 2.

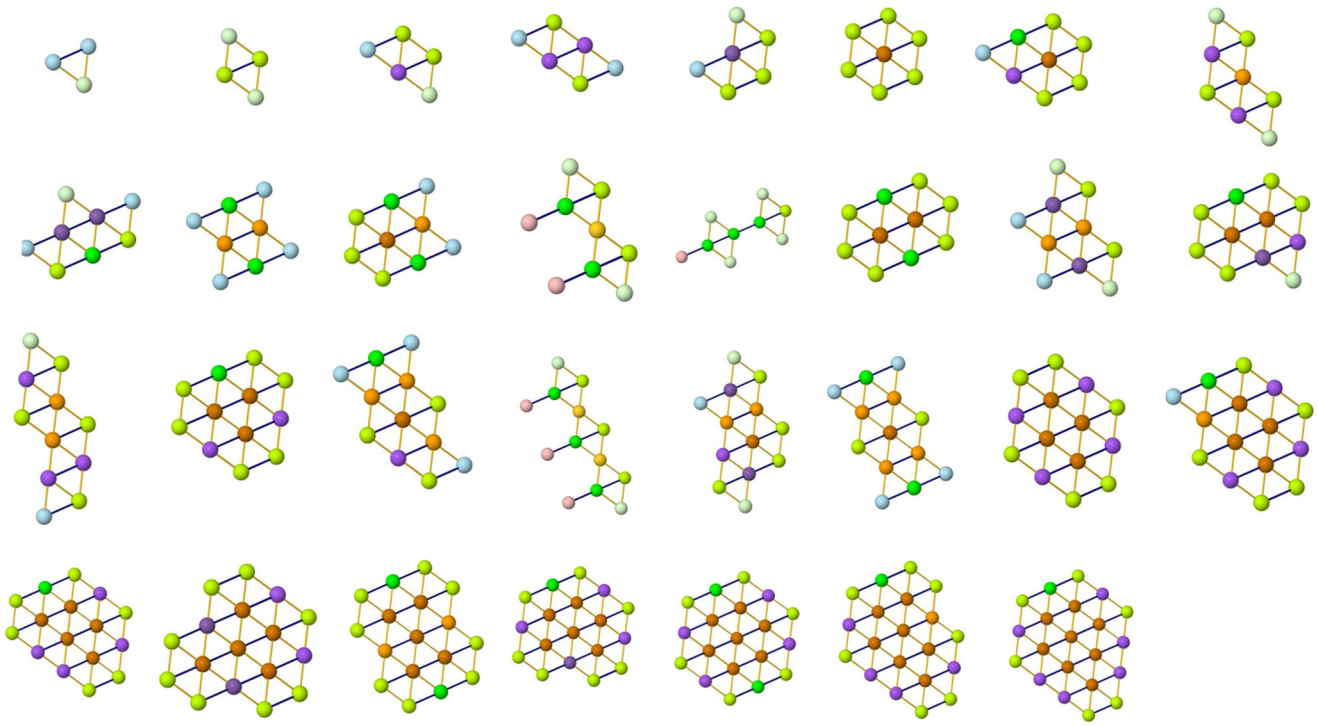

FIG. 11. Database configurations of $1/2\langle 111\rangle$ loop type in {110} habit plane, projected in the {110} plane. The same color convention is applied as in Fig. 10.

dislocation loop types were constructed for SIAs ranging from 2 to 1500. For all these configurations, we investigated the local environment of each dumbbell. To facilitate a better understanding of the neighborhood behavior in this set of configurations, the occurrence of each (n_1,n_2) pair was plotted, where n_1 refers to the number of first nearest neighbors and n_2 refers to the number of second nearest neighbors. The plotted histogram revealed that certain (n_1,n_2) pairs do not occur while other pairs are overrepresented as shown in Fig. 9.

The configurations contained in the training database of the discrete-continuum model were built in keeping with the selective dumbbell neighborhood behavior of large clusters expressed above. These configurations were constructed such that all the occurring (n_1,n_2) pairs appear in the database as well so that each occurring pair is considered for fitting.

TABLE II. DFT formation energies (expressed in eV) of smallest interstitial clusters, up to 15 interstitials, as a function of size. In this table, only the lowest formation energies are reported, at the same number of self-interstitial atoms, for the configurations used in the present database.

	Fe			W			V	
Size	C15	$1/2\langle 111\rangle$	$\langle 100\rangle$	C15	$1/2\langle 111\rangle$	$\langle 100\rangle$	C15	$1/2\langle 111\rangle$
1		4.90	5.31		10.48	12.96		2.78
2	8.03	8.63	8.33	23.71	18.40	21.31	7.99	4.80
3	11.31	11.54	12.73	27.33	25.01	28.76	9.78	6.86
4	11.28	14.48	14.32	34.35	30.79	34.81	10.75	8.00
5	14.39	17.28	17.22	42.11	36.39	41.23	13.22	9.63
6	15.85	19.80	19.70	45.34	41.52	46.59	13.71	10.86
7	17.96	21.65	21.79	53.04	45.25	53.33	16.15	11.34
8	18.76	24.22	23.74	56.29	50.44	57.26	16.59	12.87
9	20.77	26.61	27.01	62.20	55.09	62.86	18.37	13.97
10	21.70	28.29	28.96	65.96	58.49	67.89	19.04	14.49
11	22.71	30.27	30.64	69.88	62.95	72.84	19.84	15.69
12	25.55	31.77	32.70	76.84	66.23	76.83	22.04	16.20
13	26.67	35.08	35.85	80.82	73.85	84.80	22.84	18.85
14	28.55	35.09	38.37	86.13	73.64	89.21	24.16	17.84
15	29.18	37.28	39.46	90.12	77.81	92.93	25.74	18.97

Due to the compact form of clusters, there are some extra (n_1,n_2) pairs of neighbors that occur in the database. However, this is not expected to pose a problem because they do not contribute significantly in the extrapolation. The histogram of the neighborhood of the training database is shown in Fig. 9.

Database configurations were limited to 20 SIAs in 50 configurations and 22 SIAs in 31 configurations for $\langle 100\rangle$ and $1/2\langle 111\rangle$, respectively. All the training database configurations for $\langle 100\rangle$ and $1/2\langle 111\rangle$ clusters are shown in Figs. 10 and 11.

APPENDIX B

The formation energies of the small interstitial clusters, from our database, are given in Table II. The presented configurations are not necessarily those with the lowest formation energy. Moreover, it should be noted that in the case of iron, as mentioned in Sec. I, the lowest-energy configurations of small parallel clusters are $\langle 110\rangle$ and not $\langle 111\rangle$ or $\langle 100\rangle$.

[1] J. W. Gibbs, *The Scientific Papers. Volume One. Thermodynamics* (Dover, New York, 1961).

[2] M. L. Jenkins and M. A. Kirk, *Characterization of Radiation Damage by Transmission Electron Microscopy* (IOP, Bristol, 2001).

[3] Y. Matsukawa and S. J. Zinkle, Science **318**, 959 (2007).

[4] C. Domain and C. S. Becquart, Phys. Rev. B, **65**, 024103 (2001).

[5] P. M. Derlet, D. Nguyen-Manh, and S. L. Dudarev, Phys. Rev. B, **76**, 054107 (2007).

[6] C. C. Fu, F. Willaime, and P. Ordejon, Phys. Rev. Lett. **92**, 175503 (2004).

[7] D. A. Terentyev, T. P. C. Klaver, P. Olsson, M.-C. Marinica, F. Willaime, C. Domain, and L. Malerba, Phys. Rev. Lett. **100**, 145503 (2008).

[8] P. Ehrhart, K. H. Robrock, and H. R. Schober, in *Physics of Radiation Effects in Crystals*, edited by R. A. Johnson and A. N. Orlov (Elsevier, Amsterdam, 1986)

[9] C.-C. Fu, J. Dalla Torre, F. Willaime, J.-L. Bocquet, and A. Barbu, Nat. Mat. **4**, 68 (2005).

[10] M.-C. Marinica, F. Willaime, and J.-P. Crocombette, Phys. Rev. Lett. **108**, 025501 (2012).

[11] B. C. Masters, Nature (London) **200**, 254 (1963).

[12] D. A. Terentyev, L. Malerba, and M. Hou, Phys. Rev. B, **75**, 104108 (2007).

[13] S. L. Dudarev, R. Bullough, and P. M. Derlet, Phys. Rev. Lett. **100**, 135503 (2008).

[14] Z. Yao, M. L. Jenkins, M. Hernández-Mayoral, and M. A. Kirk, Philos. Mag. **90**, 4623 (2010).

[15] X. Yi, M. L. Jenkins, M. Briceno, S. G. Roberts, Z. Zhou, and M. A. Kirk, Philos. Mag. **93**, 1715 (2013).

[16] X. Yi, M. L. Jenkins, K. Hattar, P. D. Edmondson, and S. G. Roberts, Acta Mater. **92**, 163 (2015).

[17] S. L. Dudarev and P. M. Derlet, J. Phys.: Condens. Matter **17**, 7097 (2005).

[18] G. J. Ackland, M. I. Mendelev, D. J. Srolovitz, S. Han, and A. V. Barashev, J. Phys.: Condens. Matter **16**, S2629 (2004).

[19] P. A. Gordon, T. Neeraj, and M. I. Mendelev, Philos. Mag. **91**, 3931 (2011).

[20] N. Juslin and B. D. Wirth, J. Nucl. Mater. **432**, 61 (2013).

[21] L. Malerba *et al.*, J. Nucl. Mater. **406**, 19 (2010).

[22] M.-C. Marinica and F. Willaime, Solid State Phenom. **129**, 67 (2007).

[23] Y. Zhang, X.-M. Bai, M. R. Tonks, and S. B. Biner, Scr. Mat. **98**, 5 (2015).

[24] G. J. Ackland, D. J. Bacon, A. F. Calder, and T. Harry, Philos. Mag. A **75**, 713 (1997).

[25] N. Soneda and T. Diaz de la Rubia, Philos. Mag. A **78**, 995 (1998).

[26] E. Meslin, C.-C. Fu, A. Barbu, F. Gao, and F. Willaime, Phys. Rev. B **75**, 094303 (2007).

[27] C. J. Ortiz, M. J. Caturla, and C. C. Fu, F. Willaime, Phys. Rev. B **80**, 134109 (2009).

[28] D. R. Mason, X. Yi, M. A. Kirk, and S. L. Dudarev, J. Phys.: Condens. Matter **26**, 375701 (2014).

[29] J. P. Hirth and J. Lothe, *Theory of Dislocations* (McGraw-Hill, New York, 1967).

[30] D. J. Bacon, D. M. Barnett, and R. O. Scattergood, Prog. Mater. Sci. **23**, 51 (1980).

[31] E. Clouet, Philos. Mag. **89**, 1565 (2009).

[32] D. J. Bacon, R. Bullough, and J. R. Willis, Philos. Mag. **22**, 31 (1970).

[33] M. R. Gilbert, S. L. Dudarev, P. M. Derlet, and D. G. Pettifor, J. Phys.: Condens. Matter **20**, 345214 (2008).

[34] A. N. Stroh, Philos. Mag. **3**, 625 (1958).

[35] C. Varvenne, O. Mackain, and E. Clouet, Acta Mater. **78**, 65 (2014).

[36] E. Clouet, L. Ventelon, and F. Willaime, Phys. Rev. Lett. **102**, 055502 (2009).

[37] E. Clouet, Phys. Rev. B **84**, 224111 (2011).

[38] E. Clouet, L. Ventelon, and F. Willaime, Phys. Rev. B **84**, 224107 (2011).

[39] S. L. Dudarev, Philos. Mag. **83**, 3577 (2003).

[40] J. Dérè, L. Proville, and M.-C. Marinica, Acta Mater. **99**, 99 (2015).

[41] L. Dézerald, M.-C. Marinica, L. Ventelon, D. Rodney, and F. Willaime, J. Nucl. Mater. **449**, 219 (2014).

[42] J. D. Eshelby, Proc. R. Soc. London, Ser. A **241**, 376 (1957).

[43] J. D. Eshelby, Proc. R. Soc. London, Ser. A **252**, 561 (1959).

[44] M.-C. Marinica, F. Willaime, and N. Mousseau, Phys. Rev. B **83**, 094119 (2011).

[45] Y. Abe and S. Jitsukawa, Philos. Mag. **89**, 375 (2009).

[46] N. Mousseau, L. K. Béland, P. Brommer, J.-F. Joly, F. El-Mellouhi, E. Machado-Charry, M.-C. Marinica, and P. Pochet, J. Adv. At., Mol., Opt. Phys. **2012**, 925278 (2012).

[47] C. Varvenne, F. Bruneval, M.-C. Marinica, and E. Clouet, Phys. Rev. B **88**, 134102 (2013).

[48] A. Kaczmarowski, S. Yang, I. Szlufarska, and D. Morgan, Comput. Mater. Sci. **98**, 234 (2015).

[49] G. J. Ackland and R. Thetford, Philos. Mag. A **56**, 15 (1987).

[50] M.-C. Marinica *et al.*, J. Phys.: Condens. Matter **25**, 395502 (2013).
[51] G. Kresse and J. Hafner, Phys. Rev. B **47**, 558 (1993); **49**, 14251 (1994); G. Kresse and J. Furthmüller, Comput. Mater. Sci. **6**, 15 (1996); Phys. Rev. B **54**, 11169 (1996).
[52] J. Marian, B. D. Wirth, and J. M. Perlado, Phys. Rev. Lett. **88**, 255507 (2002).
[53] H. Xu, R. E. Stoller, Y. N. Osetsky, and D. Terentyev, Phys. Rev. Lett. **110**, 265503 (2013)
[54] L. K. Béland, Y. N. Osetsky, R. E. Stoller, and H. Xu, J. Alloys Compd. **640**, 219 (2015).
[55] J. Chen, N. Gao, P. Jung, and T. Sauvage, J. Nucl. Mater. **441**, 216 (2013).
[56] A. Prokhodtseva, B. Décamps, A. Ramar, and R. Schäublin, Acta Mater. **61**, 6958 (2013).
[57] T. Oppelstrup, V. V. Bulatov, A. Donev, M. H. Kalos, G. H. Gilmer, and B. Sadigh, Phys. Rev. E **80**, 066701 (2009).
[58] F. Soisson and C.-C. Fu, Phys. Rev. B **76**, 214102 (2007).
[59] M. Athènes and V. V. Bulatov, Phys. Rev. Lett. **113**, 230601 (2014).
[60] S. Moll, T. Jourdan, and H. Lefaix-Jeuland, Phys. Rev. Lett. **111**, 015503 (2013).
[61] T. Jourdan, G. Bencteux, and G. Adjanor, J. Nucl. Mater. **444**, 298 (2014).
[62] L. Messina, M. Nastar, T. Garnier, C. Domain, and P. Olsson, Phys. Rev. B **90**, 104203 (2014).